# Mixed finite element method for linear elasticity in a cracked domain

M.A. Bennani[a,*], Abdeslam El Akkad[b], Ahmed Elkhalfi[a]
[a]Facultée des Sciences et Techniques de Fès, Maroc.
[b]Centre Régional des Métiers d'Education et de Formation Fès, Annexe Sefrou, Maroc.

*Abstract*: - A mixed finite element procedure for plane elasticity system in a cracked domains is introduced and analyzed. There is a member of the family for each polynomial degree, beginning with degree two for the stress and degree one for the displacement, and each is stable and affords optimal order approximation. The simplest element pair involves 24 local degrees of freedom for the stress and 6 for the displacement. We also construct a lower order element involving 21 stress degrees of freedom and 3 displacement degrees of freedom which is, we believe, likely to be the simplest possible conforming stable element pair with polynomial shape functions.

The mixed formulation is used in elasticity for incompressible materials such as rubber, its use for linear elasticity has been discussed by many researchers, in this section we will study the compatibility of the mixed formulation cracked domains and compare it with the conventional method.The numerical results are compared with some previously published works or with others coming from commercial code.

**Keywords:** Elasticity problem; mixed finite element method; Lower order element; linear fracture mechanics,

## 1.Introduction

Mixed finite element methods for linear elasticity are based on approximations of a stress-displacement system derived from the Hellinger-Reissner variational principle **[7]**, in which both displacements and stresses were approximated simultaneously.

For $\boldsymbol{k = 1}$ the stress element is fairly complicated, involving 24 degrees of freedom on each triangle. A slightly simpler element, in which the displacement is sought as a piecewise rigid motion (3 degrees of freedom per triangle), and the stress space involves 21 degrees of freedom per triangle, was also shown to be stable. This method is first order in both stress and displacement.

much more difficult to construct. The first class of inf-sup stable methods were the so called composite elements **[4, 5].**

As mentioned, conforming mixed finite elements for elasticity tend to be quite complicated. The earliest elements, which worked only in two dimensions, used composite elements for stress **[11, 12].** Much

$$\boldsymbol{\nabla.\sigma + f = 0 \; in \; \Omega} \qquad \textbf{(1)}$$

$$\boldsymbol{\sigma.n = \bar{t} \; on \; \Gamma_t} \qquad \textbf{(2)}$$

$$\boldsymbol{\sigma.n = 0 \; on \; \Gamma_{c^+}} \qquad \textbf{(3)}$$

$$\boldsymbol{\sigma.n = 0 \; on \; \Gamma_{c^-}} \qquad \textbf{(4)}$$

more recently, elements using polynomial shape functions were developed for simplicial meshes in two [14] and three dimensions **[16, 17]** and for rectangular meshes **[14, 15].** Heuristics given in **[13]** and **[16]** indicate that it is not possible to construct significantly simpler elements with polynomial shape functions and which preserve both the conformity and symmetry of the stress.

Many mixed finite element methods have been developed for plane elasticity, and generally speaking, they can be grouped into two categories: methods that enforce the symmetry of the stress weakly, and methods that enforce the symmetry exactly (strongly). In the former category, the stress tensor is not necessarily symmetric, but rather orthogonal to anti-symmetric tensors up to certain moments. Weakly imposed stress symmetry methods also introduce a new variable into the formulation that approximates the anti-symmetric part of the gradient of u; see for example **[2, 3].** On other hand, exactly symmetric stress methods have been

Section **2** presents the model problem used in this paper. The discretization by mixed finite elements described is in section **3**. Error analysis described is in section **4**. In section **5**, numerical experiments within the framework of this publication were carried out.

## 2.Governing equations of linear elasticity

The equilibrium equations and boundary conditions are

The system of (anisotropic, inhomogeneous) linear elasticity consists of the constitutive equations:

$$\boldsymbol{\sigma = C : \varepsilon} \qquad \textbf{(5)}$$

where C is the Hooke tensor, C is assumed here to have constant coefficients. Its inverse (compliance tensor) will be denoted by E. Hence

$$\boldsymbol{\sigma} = \boldsymbol{C}:\boldsymbol{\varepsilon} \Leftrightarrow \boldsymbol{\varepsilon} = \boldsymbol{E}:\boldsymbol{\sigma}. \quad (6)$$

For a homogeneous isotropic medium and for $\tau$ symmetric we have

$$\boldsymbol{C_\tau} = 2\boldsymbol{\mu\tau} + \boldsymbol{\lambda tr(\tau)\delta},$$

where $\boldsymbol{\delta}$ is the unit (identity) second-order tensor and $\boldsymbol{\lambda} \geq \mathbf{0}$ and $\boldsymbol{\mu} \geq \mathbf{0}$ are the Lamé constants.

The trace operator applied to a tensor $\boldsymbol{\tau}$ is given by $\boldsymbol{tr(\tau)} = \boldsymbol{\tau_{11}} + \boldsymbol{\tau_{22}} = \boldsymbol{\tau}:\boldsymbol{\delta}$.

We consider small strains and displacements. The kinematics equations therefore consist of the strain-displacement relation

$$\boldsymbol{\varepsilon} = \boldsymbol{\varepsilon(u)} = \boldsymbol{\nabla_s u} \quad (7)$$

where $\boldsymbol{\nabla_s u} = \frac{1}{2}(\boldsymbol{\nabla u} + \boldsymbol{\nabla u^T})$ is the symetric part of the the gradient operator, and the boundary conditions

$$\boldsymbol{u} = \overline{\boldsymbol{u}} \ \boldsymbol{on} \ \boldsymbol{\Gamma_u} \quad (8)$$

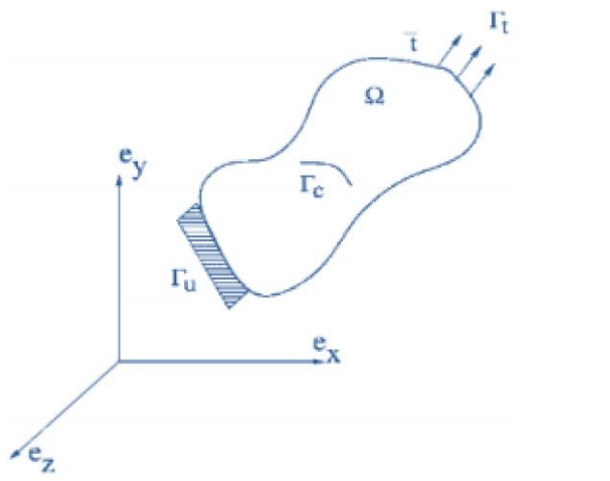


FIG. 1 : BODY WITH INTERNAL BOUNDARY SUBJECTED TO LOADS.

We set

$$\boldsymbol{H(div,\Omega)} = \{\boldsymbol{\sigma}|\boldsymbol{\sigma} \in (\boldsymbol{L^2(\Omega)})^{2^2}; \ \boldsymbol{\sigma_{ij}} = \boldsymbol{\sigma_{ji}} \ \forall \boldsymbol{i,j}; \boldsymbol{div\sigma} \in (\boldsymbol{L^2(\Omega)})^2\}, \quad (9)$$

which is a Hilbert space under the norm

$$\|\boldsymbol{\sigma}\|_{\boldsymbol{H(div,\Omega)}} = (\|\boldsymbol{\sigma}\|^2 + \|\boldsymbol{\nabla.\sigma}\|^2)^{\frac{1}{2}}$$

And we set

$$\boldsymbol{H_g(div,\Omega)} = \{\boldsymbol{\tau} \in \boldsymbol{H(div,\Omega)}; \ \boldsymbol{\tau.n} = \boldsymbol{g} \ \boldsymbol{on} \ \boldsymbol{\Gamma_t}\} \quad (10)$$

$$\boldsymbol{L^2_{dis}(\Omega)} = \{\boldsymbol{u} \in (\boldsymbol{L^2(\Omega)})^2, \boldsymbol{u} \ \boldsymbol{discontinuous} \ \boldsymbol{on} \ \boldsymbol{\Gamma_C}\}. \quad (11)$$

Then the standard weak formulation of the equilibrium equations is the following:

Find $\boldsymbol{\sigma} \in \boldsymbol{H_{\bar{t}}(div,\Omega)}$ and $\boldsymbol{u} \in \boldsymbol{L^2_{dis}(\Omega)}$ such that :

$$\int_{\boldsymbol{\Omega}} (\boldsymbol{E}:\boldsymbol{\sigma}):\boldsymbol{\tau dx} + \int_{\boldsymbol{\Omega}} \boldsymbol{u.div\tau dx} = \int_{\boldsymbol{\Gamma_u}} \overline{\boldsymbol{u}}\boldsymbol{\tau.n d\Gamma} \ \forall \boldsymbol{\tau} \in \boldsymbol{H_0(div,\Omega)} \quad (12)$$

$$\int_{\boldsymbol{\Omega}} \boldsymbol{v.div\sigma dx} + \int_{\boldsymbol{\Omega}} \boldsymbol{f.v dx} = \mathbf{0} \ \forall \boldsymbol{v} \in \boldsymbol{L^2_{dis}(\Omega)}. \quad (13)$$

For a matrix field $\boldsymbol{\tau}$, $div\tau$ is the vector obtained by applying the divergence operator row-wise

$$\boldsymbol{div\tau} = (\frac{\boldsymbol{\partial \tau_{11}}}{\boldsymbol{\partial x}} + \frac{\boldsymbol{\partial \tau_{12}}}{\boldsymbol{\partial y}}, \frac{\boldsymbol{\partial \tau_{21}}}{\boldsymbol{\partial x}} + \frac{\boldsymbol{\partial \tau_{22}}}{\boldsymbol{\partial y}}),$$

and the colon denotes the scalar product

$$\boldsymbol{\sigma}:\boldsymbol{\tau} = \sum_{\boldsymbol{i,j=1}}^{\boldsymbol{2}} \boldsymbol{\sigma_{ij}\tau_{ij}}.$$

Let the bilinear forms a and b, and the linear forms l and s such that:

$$\boldsymbol{a(\sigma,\tau)} = \int_{\boldsymbol{\Omega}} (\boldsymbol{E}:\boldsymbol{\sigma}):\boldsymbol{\tau dx} \quad (14)$$

$$\boldsymbol{b(\sigma,u)} = \int_{\boldsymbol{\Omega}} \boldsymbol{u.div\sigma dx} \quad (15)$$

$$\boldsymbol{l(v)} = -\int_{\boldsymbol{\Omega}} \boldsymbol{f.v dx} \quad (16)$$

$$\boldsymbol{s(\tau)} = \int_{\boldsymbol{\Gamma_u}} \overline{\boldsymbol{u}}\boldsymbol{\tau.n d\Gamma}, \boldsymbol{for\ all\ \tau} \in \boldsymbol{H(div,\Omega)}. \quad (17)$$

The underlying weak formulation (12)-(13) may be restated as:

Find $\boldsymbol{\sigma} \in \boldsymbol{H_{\bar{t}}}$ and $\boldsymbol{u} \in \boldsymbol{L^2_{dis}(\Omega)}$ such that :

$$\boldsymbol{a(\sigma,\tau)} + \boldsymbol{b(\tau,u)} = \boldsymbol{s(\tau)}, \ \boldsymbol{for\ all\ \tau} \in \boldsymbol{H_0(div,\Omega)} \quad (18)$$

$$\boldsymbol{b(\sigma,v)} = \boldsymbol{l(v)}, \boldsymbol{for\ all\ v} \in \boldsymbol{L^2_{dis}(\Omega)}. \quad (19)$$

**Theorem 1.** Let $\boldsymbol{E}$ and $\boldsymbol{\Psi}$ be real Hilbert spaces, $\boldsymbol{a(\xi_1,\xi_1)}$ a bilinear form on $\boldsymbol{E \times E}$, and $\boldsymbol{b(\xi,\psi)}$ a bilinear form an $\boldsymbol{E \times \Psi}$. Set

$$K = \{\xi | \xi \in E, b(\xi, \psi) = 0 \ \forall \psi \in \Psi\}, \quad (20)$$

and assume that:

$$\exists \alpha > 0, s.t. a(\xi, \xi) \geq \alpha \|\xi\|_E^2 , \forall \xi \in K \quad (21)$$

$$\exists \beta > 0, s.t. \sup_{\xi \in E - \{0\}} \frac{b(\xi, \psi)}{\|\xi\|_E^2} \geq \beta \|\xi\|_\Psi \ , \forall \psi \in \Psi, \quad (22)$$

Then for every $l_1 \in E'$ and $l_2 \in \Psi'$ there exists a unique solution $(\overline{\xi}, \overline{\psi})$ of the problem :

$$a(\overline{\xi}, \overline{\xi}) + b(\xi, \overline{\psi}) = \langle l_1, \xi \rangle, for\ all\ \psi \in E, \quad (23)$$

$$b(\overline{\xi}, \psi) = \langle l_2, \psi \rangle, for\ all\ \psi \in \Psi. \quad (24)$$

**REMARK 1.** It is clear that if $a(\xi_1, \xi_2)$ is symmetric, the solution $(\overline{\xi}, \overline{\psi})$ of **(21)-(22)** minimizes the functional

$$J(\xi) = \frac{1}{2} a(\xi, \xi) - \langle l_1, \xi \rangle \quad (25)$$

on the subspace of **E,**

$$K(l_2) = \{\xi |\ \xi \in E, b(\xi, \psi) = \langle l_2, \psi \rangle \ \forall \psi \in \Psi\}, \quad (26)$$

and the formulation **(21)-(22)** corresponds to the introduction in **(25)-(26)** of the Lagrange multiplier $\overline{\xi}$**.**

## 3.Mixed finite element approximation

Let $T_h; h > 0$**,** be a family of rectangulations of **Ω.** The edges of elements will be denoted $e_i$ ***(i=1, 2, 3 or i=1, 2, 3, 4)*** in the two-dimensional case.

Let us deal first with the abstract framework **(21)-(22).** Assume that we are given two sequences $\{E_h\}_{h>0}$ and $\{\Psi_h\}_{h>0}$ of subspaces $E$ and $\Psi$, respectively. We set

$$K_h = \{\xi_h | \xi_h \in E_h, b(\xi_h, \psi_h) = 0 \forall \psi_h \in \Psi_h\}, \quad (27)$$

We have the following approximation theorem

**Theorem 2.** Assume that

$$\exists \alpha_h > 0, s.t. a(\xi, \xi) \geq \alpha_h \|\xi\|_E^2 \quad \forall \xi \in K_h \quad (28)$$

$$\exists \beta_h > 0, s.t. \sup_{\xi \in E_h - \{0\}} \frac{b(\xi, \psi)}{\|\xi\|_E} \geq \beta_h \|\psi\|_\Psi \quad \forall \psi \in \Psi_h. \quad (29)$$

has a unique solution. Moreover, there exists a constant $\gamma_h(\alpha_h, \beta_h) > 0$ such that

$$a(\overline{\xi}_h, \overline{\xi}) + b(\xi, \overline{\psi}_h) = \langle l_1, \xi \rangle, for\ all\ \xi \in E_h, \quad (30)$$

$$b(\overline{\xi}_h, \psi) = \langle l_2, \psi \rangle, for\ all\ \psi \in \Psi_h \quad (31)$$

Then for every $l_1 \in E'$ and $l_2 \in \Psi'$, and for every $h > 0$, the discrete problem

$$\|\overline{\xi} - \overline{\xi}_h\|_E + \|\overline{\psi} - \overline{\psi}_h\|_\Psi \leq \gamma_h ( \inf_{\xi_h \in E_h} \|\overline{\xi} - \xi_h\|_E + \inf_{\psi_h \in \Psi_h} \|\overline{\psi} - \psi_h\|_\Psi ). \quad (32)$$

The dependence of $\gamma_h$ on$\alpha_h$ and $\beta_h$ can be easy traced **[8].** Clearly if **(21)** and **(22)** hold with constants $\overline{\alpha}$ and $\overline{\beta}$ independent of **h**, then **(32)** holds with a constant $\overline{\gamma}$ independent of h.

To give a more precise definition of our mixed finite element approximation we shall need a few definitions. Let us define on an element **T**

Let **k** a positive integer. For a single triangle **T** we define spaces of shape functions

$$\Sigma_T = P_{k+1}(T, S) + \{\tau \in P_{k+2}(T, S) / div \tau = 0\} = \{\tau \in P_{k+2}(T, S) / div \tau \in P_k(T, \mathbb{R}^2)\} \quad (33)$$

Here **S** denotes the 3-dimensional vectorspace of $2 \times 2$ symmetric matrices, in which the stress field takes it's values.

Let:

$$V_T = P_k(T, \mathbb{R}^2), \quad (34)$$

$P_k(X, Y)$**:** the space of polynomials on **X** of degree at most **k** taking values in **Y.**

Clearly

$$dim V_T = (k + 1)(k + 2). \quad (35)$$

For **k=1**, the space $V_T$ has dimension 6 and a complete set of degrees of freedom are given by the value of the two components at the three nodes interior to **T**. The space $\Sigma_T$ clearly has dimension at least **24**, since the $dim P_3(T, S) = 30$ and the condition that $div \tau \in P_1(T, \mathbb{R}^2)$ represents six linear constraints.

In [18] it is shown that

$$\boldsymbol{dim\Sigma_T = (3k^2 + 17k + 28)/2.} \quad \textbf{(36)}$$

and that a unisolvent set of local degrees of freedom is given by

- the values of three components of $\boldsymbol{\tau(x)}$ at each vertex **x** of **T** (9 degrees of freedom)
- the values of the moments of degree at most **k** of the two normal components of $\boldsymbol{\tau}$ on each edge **e** of **T** (**6k + 6** degrees of freedom)
- the value of the moments $\int_T \boldsymbol{\tau}:\boldsymbol{\varphi dx}$, $\boldsymbol{\varphi} \in \boldsymbol{N_k(T)}$ $\boldsymbol{((3k^2 + 5k - 2)/2}$ degrees of freedom)

Here

$$\boldsymbol{N_k(T) = \varepsilon[P_k(T, \mathbb{R}^2)] + J(b_T^2 P_{k-2}(T, \mathbb{R}))}. \quad \textbf{(37)}$$

Where $\boldsymbol{\varepsilon}$ is the infinitesimal strain operator (symmetrized gradient), $\boldsymbol{b_T}$ is the cubic bubble function on **T** (the unique cubic polynomial achieving a maximum value of unity on **T** and vanishing on $\boldsymbol{\partial T}$), and **J** is Airy stress operator

$$\boldsymbol{\tau = Jq} := \begin{pmatrix} \dfrac{\partial^2 q}{\partial^2 y} & -\dfrac{\partial^2 q}{\partial x \partial y} \\ -\dfrac{\partial^2 q}{\partial x \partial y} & \dfrac{\partial^2 q}{\partial^2 x} \end{pmatrix} \quad \textbf{(38)}$$

Note that, on $\boldsymbol{\partial\Omega}$

$$\boldsymbol{J(q)n.n} = \frac{\partial^2 q}{\partial^2 t}, \ \boldsymbol{J(q)n.t} = -\frac{\partial^2 q}{\partial t \partial n},$$

where **n** and **t** are the unit normal and tangent vectors to $\boldsymbol{\partial\Omega}$, respectively.

Note that when **k = 0,** $\boldsymbol{N_k(T)}$ is simply the space of constant tensors.

The associated finite element element space $\boldsymbol{V_h}$ is then the space of all piecewise linear vector fields with respect to this triangulation, not subject to any interelement continuity conditions. The space $\boldsymbol{\Sigma_h}$ is the space of all matrix fields which belong piecewise to $\boldsymbol{\Sigma_T}$, subject to the continuity conditions that the normal components are continuous across mesh edges and all components are continuous at mesh vertices.

The Hellinger-Reissner variational principle characterizes the stress field $\boldsymbol{\sigma}$ and the displacement field u engendered in a planar linearly elastic body occupying a region $\boldsymbol{\Omega}$ by a body load f as the unique critical point of the functional $\boldsymbol{\Lambda : H(div, \Omega, S) \times L^2(\Omega, \mathbb{R}^2) \to \mathbb{R}}$ defined by

Here the compliance tensor $\boldsymbol{A = A(x)}: \boldsymbol{S \to S}$ is bounded and symmetric positive definite uniformly

$$\boldsymbol{\Lambda(\tau, v)} = \int_{\boldsymbol{\Omega}} (\frac{1}{2}\boldsymbol{A\tau}:\boldsymbol{\tau} + \boldsymbol{div\tau}.\boldsymbol{v} - \boldsymbol{f}.\boldsymbol{v})\boldsymbol{dx}. \quad \textbf{(39)}$$

for $\boldsymbol{x \in \Omega}$, and the critical point is sought among all $\boldsymbol{\tau \in H(div, \Omega, S)}$, the space of square-integrable symmetric matrix fields with square-integrable divergence, and all $\boldsymbol{v \in L^2(\Omega, \mathbb{R}^2)}$, the space of square-integrable vector fields.

To ensure that a unique critical point of the Hellinger-Reissner functional $\boldsymbol{\Lambda}$ exist and that it provides a good approximation of the true solution, they must satisfy the stability conditions:

(A1) $\boldsymbol{div\Sigma_h \subset V_h}$.

(A2) There exists a linear operator $\boldsymbol{\prod_h : H^1(\Omega, S) \to \Sigma_h}$, boundedin $\boldsymbol{£(H^1, L^2)}$ uniformly with respect to h, and such that $\boldsymbol{div \prod_h \sigma = P_h div\sigma}$ for all $\boldsymbol{\sigma \in H^1(\Omega, S)}$, where $\boldsymbol{P_h: L^2(\Omega, \mathbb{R}^2) \to V_h}$ denotes the $\boldsymbol{L^2}$-projection.

There is a variant of the lowest degree **(k = 1)** element involving fewer degrees of freedom. For this we take $\boldsymbol{V_T}$ to be the space of infinitesimal rigid motions on T , i.e., the span of the constant vectorfields and the linear vectorfield $\boldsymbol{(-x_2, x_1)}$.

Then for **k=1** we choose

$$\boldsymbol{\Sigma_T = \{\tau \in P_3(T, S)/div\tau \in P_1(T, \mathbb{R}^2)\}}. \quad \textbf{(40)}$$

We then have $\boldsymbol{dim\Sigma_T = 24}$ and $\boldsymbol{dimV_T = 6}$. The element diagram is shown in **Figure 2**.

All of our discretizations of $\boldsymbol{H(div\Omega, S)}$ involve vertex degrees of freedom. In this respect, they differ from the usual mixed elements for scalar elliptic problems, such as the Raviart-Thomas elements. As mentioned earlier, continuity at the vertices is not required for functions belonging to $\boldsymbol{H(div\Omega, S)}$. Moreover, it impedes the implementation of the elements using interelement Lagrange multipliers as in [20].

Just as the conforming element shown on the left of Figure 2 can be simplified to element of Figure 4. The displacement space consists of piecewise rigid motions, and the stress space is reduced by adding the restriction that the divergence be a rigid motion on each triangle.

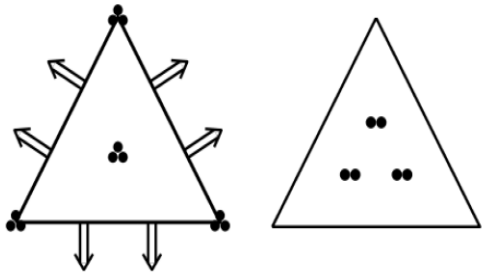

FIG. 2- Element diagrams for the conforming elements in the cases k = 1.

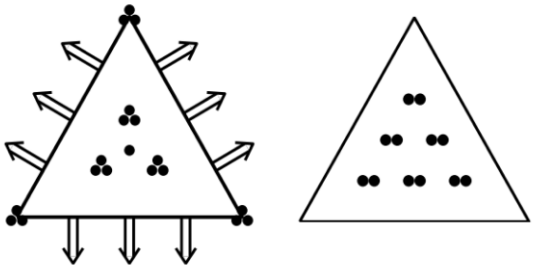

FIG. 3- Element diagrams for the conforming elements in the cases k = 2.

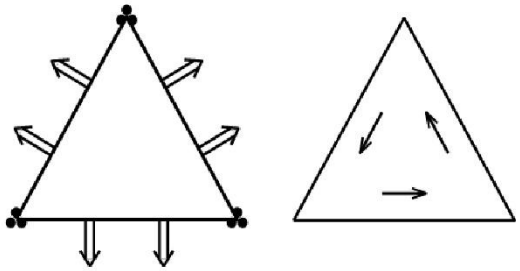

FIG. 4- A simplified element pair.

We define a space

$$\boldsymbol{\Sigma_h} = \{\boldsymbol{\tau_h} \in \boldsymbol{H(div,\Omega)}, \boldsymbol{\tau_h}|_T \in \boldsymbol{\Sigma_T} \forall \boldsymbol{T} \in \boldsymbol{T_h}\} \quad \textbf{(41)}$$

and the space

$$\boldsymbol{V_h} = \{\boldsymbol{v_h} \in \boldsymbol{L^2_{dis}(\Omega)}, \boldsymbol{v_h}|_T \in \boldsymbol{P_1(T,\mathbb{R}^2)} \forall \boldsymbol{T} \in \boldsymbol{T_h}\}. \quad \textbf{(42)}$$

We chose finite-dimensional subspace $\boldsymbol{H_0^h(div,\Omega)} \subset \boldsymbol{H_0(div,\Omega)}$.

A mixed finite element approximation of (12)-(13) is defined by

Find $\boldsymbol{\sigma_h} \in \boldsymbol{\Sigma_h}$ and $\boldsymbol{u_h} \in \boldsymbol{V_h}$ such that

$$\int_{\Omega} (\boldsymbol{E}:\boldsymbol{\sigma_h}):\boldsymbol{\tau_h} \boldsymbol{dx} + \int_{\Omega} \boldsymbol{u_h}.\boldsymbol{div}\boldsymbol{\tau_h} \boldsymbol{dx} = \int_{\Gamma_u} \overline{\boldsymbol{u}}\boldsymbol{\tau_h}.\boldsymbol{n} \boldsymbol{d\Gamma} \ \forall \boldsymbol{\tau_h} \in \boldsymbol{H_0^h(div,\Omega)} \quad \textbf{(43)}$$

$$\int_{\Omega} \boldsymbol{v_h}.\boldsymbol{div}\boldsymbol{\sigma_h} \boldsymbol{dx} + \int_{\Omega} \boldsymbol{f}.\boldsymbol{v_h} \boldsymbol{dx} = \boldsymbol{0} \ \forall \boldsymbol{v_h} \in \boldsymbol{V_h}. \quad \textbf{(44)}$$

We obtain a system of linear equations

$$\begin{pmatrix} \boldsymbol{A} & \boldsymbol{B^T} \\ \boldsymbol{B} & \boldsymbol{0} \end{pmatrix} \begin{pmatrix} \boldsymbol{T} \\ \boldsymbol{U} \end{pmatrix} = \begin{pmatrix} \boldsymbol{G} \\ \boldsymbol{F} \end{pmatrix} \quad \textbf{(45)}$$

where $\boldsymbol{G} = [\boldsymbol{s_m}]$ and $\boldsymbol{F} = [\boldsymbol{l_m}]$

$l$ and s are defined in (16) and (17) respectively.

The matrix associated for the system (45) is symmetric indefinite. We use the iterative methods Minimum Residual Method (MINRES) for solving the symmetric system.

## 4.Error analysis

Having established the stability properties **(A1)** and **(A2)** for the spaces $\boldsymbol{\Sigma_h}$ and $\boldsymbol{V_h}$, we conclude that the Hellinger-Reissner functional $\boldsymbol{\Lambda}$ has a unique critical point $(\boldsymbol{\sigma_h}, \boldsymbol{u_h})$ over $\boldsymbol{\Sigma_h} \times \boldsymbol{V_h}$, i.e., the mixed method is well-defined.

**Theorem 3.** If $(\boldsymbol{\sigma}, \boldsymbol{u})$ is the solution of **(12)-(13)** and $(\boldsymbol{\sigma_h}, \boldsymbol{u_h})$ is the solution of **(30)-(31),** there exist a constant $\boldsymbol{C} > \boldsymbol{0}$ such that:

**REMARK 2.** More technical arguments allow us to

$$\|\boldsymbol{\sigma} - \boldsymbol{\sigma_h}\|_{\boldsymbol{H(div)}} + \|\boldsymbol{u} - \boldsymbol{u_h}\|_{\boldsymbol{L^2}} \leq \boldsymbol{C} \inf_{\boldsymbol{\tau} \in \boldsymbol{\Sigma_h}, \boldsymbol{v} \in \boldsymbol{V_h}} (\|\boldsymbol{\sigma} - \boldsymbol{\tau}\|_{\boldsymbol{H(div)}} + \|\boldsymbol{u} - \boldsymbol{v}\|_{\boldsymbol{L^2}}). \quad \textbf{(46)}$$

avoid the regularity assumption $\boldsymbol{div\sigma} \in (\boldsymbol{L^2(\Omega)})^{\boldsymbol{2}}$. In this case $\boldsymbol{\sigma} \in \boldsymbol{H(div,\Omega)}$.

The following theorem, which is proven in **[13],** gives an error estimate.

**Theorem 4.** Let $(\boldsymbol{\sigma}, \boldsymbol{u})$ is the unique critical point of the Hellinger-Reissner functional over $\boldsymbol{H(div\Omega, S)} \times \boldsymbol{L^2(\Omega, \mathbb{R}^2)}$ , and let $(\boldsymbol{\sigma_h}, \boldsymbol{u_h})$ is the unique critical point over $\sum_{\boldsymbol{h}} \times \boldsymbol{V_h}$, where $\sum_{\boldsymbol{h}}$ and $\boldsymbol{V_h}$ are the spaces defined above for some integer $\boldsymbol{k \geq 1}$.

Then :

$$\|\boldsymbol{\sigma}-\boldsymbol{\sigma}_h\|_0 \le ch^m\|\boldsymbol{\sigma}\|_m, 1 \le m \le k+2, \quad (47)$$

$$\|div\boldsymbol{\sigma}-div\boldsymbol{\sigma}_h\|_0 \le ch^m\|div\boldsymbol{\sigma}\|_m, 0 \le m \le k+1, \quad (48)$$

$$\|\boldsymbol{u}-\boldsymbol{u}_h\|_0 \le ch^m\|\boldsymbol{u}\|_{m+1}, 1 \le m \le k+1. \quad (49)$$

For this element pair defined in (40), we have

$$\|\boldsymbol{\sigma}-\boldsymbol{\sigma}_h\|_0 \le ch^m\|\boldsymbol{\sigma}\|_m, 1 \le m \le 2, \quad (50)$$

$$\|div\boldsymbol{\sigma}-div\boldsymbol{\sigma}_h\|_0 \le ch^m\|div\boldsymbol{\sigma}\|_m, 0 \le m \le 1, \quad (51)$$

$$\|\boldsymbol{u}-\boldsymbol{u}_h\|_0 \le ch\|\boldsymbol{u}\|_2. \quad (52)$$

## 5.The linear fracture mechanics

In short, the linear fracture mechanics is the study of the effect of the presence of a crack in a solid subjected to different types of loading, its purpose is to predict when, how and where would propagate the crack. We shrunk the assumption of small perturbation **(PPH)** and quasi-static evolution of cracks and it would uses the assumption of plane strain.

$$\boldsymbol{J} = \lim_{\Gamma\to 0}\int_{\Gamma} \boldsymbol{n}.\boldsymbol{H}.\boldsymbol{q}\, d\Gamma \quad (54)$$

There are three primary forms of crack width, shown in Fig.5. One can clearly distinguish the mode I, where the displacement is in the same direction as the force exerted is the most dangerous mode. That is why we are particularly interested.

Modes of crack opening:

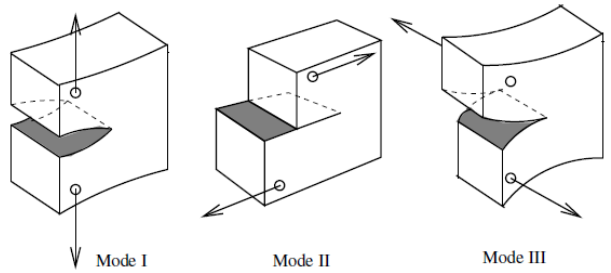


FIG. 5- Crack Modes

The prediction of the propagation of a crack, necessarily involves the calculation of the stress intensity near the crack tip. However, the crack propagation depends on not only the loading but also the geometry, size and location of the crack, which is why we use the stress intensity factor K that takes into account all its features. To facilitate the prediction of whether or not the propagation of the crack in the field of study. Several scientific research had addressed the problem of the cracking, and were able to establish the formulas, and analytical approximation of the stress intensity factor, for relatively simple test cases.

### 5.1. Analytical compute of stress intensity factor

We can calculate the stress intensity for the three modes of cracking factor; in general, we calculate the stress intensity factor by the following formulation:

$$\boldsymbol{K_j} = \boldsymbol{\sigma}.\sqrt{\boldsymbol{\pi}.\boldsymbol{a}}.\boldsymbol{f_j} \quad (53)$$

Where "**σ"** is the stress applied to the overall structure, "**a"** the length of the crack and "$\boldsymbol{f_j}$" is the correction factor taking into account the shape of the crack geometry and structure.

### 5.2. Numerical compute of stress intensity factor

The most used parameter in linear fracture mechanics [21] to characterize a crack is the *J*-integral. *J*-integral predicts initiation, propagation and instability of a crack in ductile materials. According to [22,23] the *J*-integral is independent of the path followed and the geometry of the domain, it depends mainly the change in potential energy at an advanced crack. In the context of quasi-static analysis the J-integral [24] is defined in two dimensions as:

Where $\Gamma$ is a contour beginning on the bottom crack surface and ending on the top surface, as shown in **(FIG.6)** ; the limit $\boldsymbol{\Gamma \to 0}$ indicates that **Γ** shrinks on to the crack tip; $\boldsymbol{q}$ is a unit vector in the virtual crack extension direction; and $\boldsymbol{n}$ is the outward normal to **Γ. *H*** is given by

$$\boldsymbol{H} = \boldsymbol{W}.\boldsymbol{I} - \boldsymbol{\sigma}.\frac{\partial \boldsymbol{u}}{\partial \boldsymbol{X}} \quad (55)$$

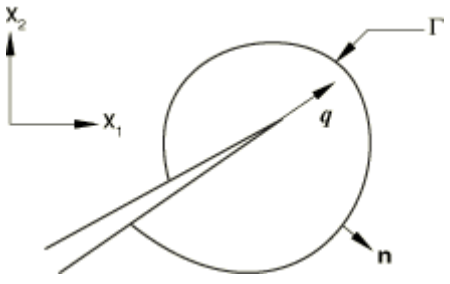


FIG. 6- Contour for evaluation of the J-integral.

For elastic material behavior $\boldsymbol{W}$ is the elastic strain energy; for elastic-plastic or elastic-viscoplastic material behavior $\boldsymbol{W}$ is defined as the elastic strain energy density plus the plastic dissipation, thus representing the strain energy in an "equivalent elastic material." This implies that the *J*-integral calculation is suitable only for monotonic loading of elastic-plastic materials. In linear elasticity, the J-integral is the energy of Griffith.

$$\boldsymbol{J = G} \qquad \textbf{(56)}$$

$$\boldsymbol{J = \frac{(K_I^2 + K_{II}^2)(1 - v^2)}{E^*} + \frac{1 + v}{E} K_{III}^2} \qquad \textbf{(57)}$$

In plane stress $\boldsymbol{E^* = E}$

In Plane strain $\boldsymbol{E^* = \frac{E}{1-v^2}}$

From equation **(57)** we could deduce the stress intensity factor for different mode cracking $(K_I, K_{II}, K_{III})$.

## 6.Numerical simulation

In this section some numerical results of calculations with mixed finite element Method and commercial code will be presented. Using our solver, we run Crack in a rectangular plate subjected to uniaxial tension **[3]** with a number of different model parameters.

### 6.1. Numerical test 1: convergence rate

We will study the numerical convergence of a cracked plate subjected to a linear load, in our case, the fissure is inclined at an angle of $45^o$. Is named "h" the height of the plate and "b" its width, while "2a" is the length of the crack.

The purpose of this study is to make a comparison between the convergence results for the standard finite element and mixed finite elements, to make it will vary the mesh size from largest to smallest and take as output value displacement. Then we can compare the two methods and conclude the results.

Let the numerical test data:

| | |
|---|---|
| $h$ | 10 |
| $b$ | 10 |
| $a$ | 1 |
| $\sigma$ | $1(SI)$ |
| Material: Young's modulus | 100 (SI) |
| and Poisson's ratio | 0.3 |

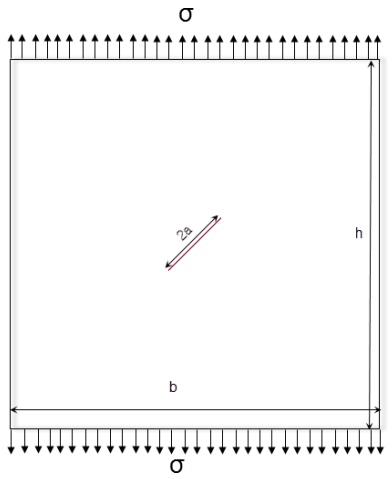


FIG. 7- Numerical Test for a cracked plate subjected to a linear load

*Results*

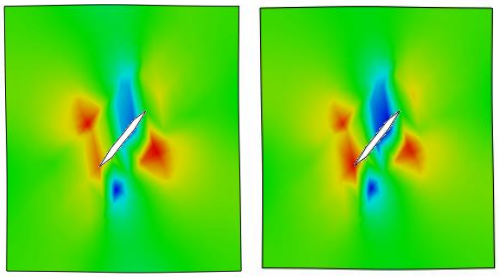

FIG. 8- Stress obtained with Max Size of Mesh By Mixed Finite Element Method (Left) And classical Finite Element Method (Right).

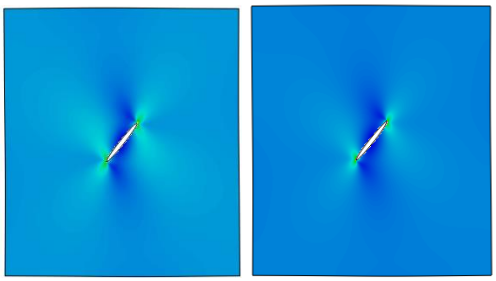

FIG. 9- Stress obtained with Minimum Size of mesh By Mixed Finite Element Method (Left) And classical Finite Element Method (Right).

From these results, we can see a distribution of stress field quite similar, it is clear that a coarse mesh gives bad results while a fine mesh gives very good results, however, a fine mesh takes longer that a coarse mesh. Which lead us to search for the optimal mesh that gives relatively accurate results but also consume less resource by its speed.

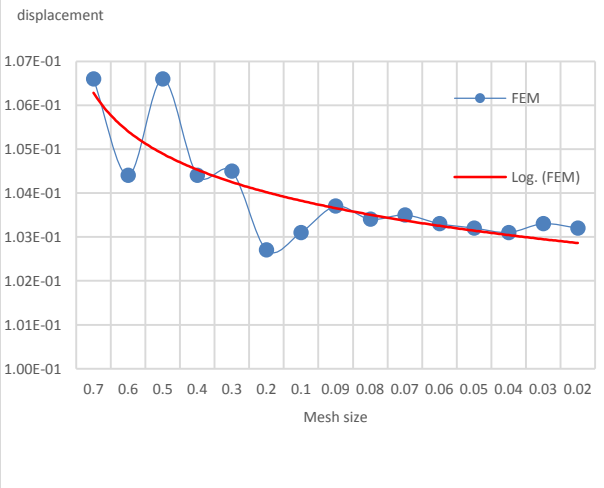


FIG. 10- Convergence rate for FEM.

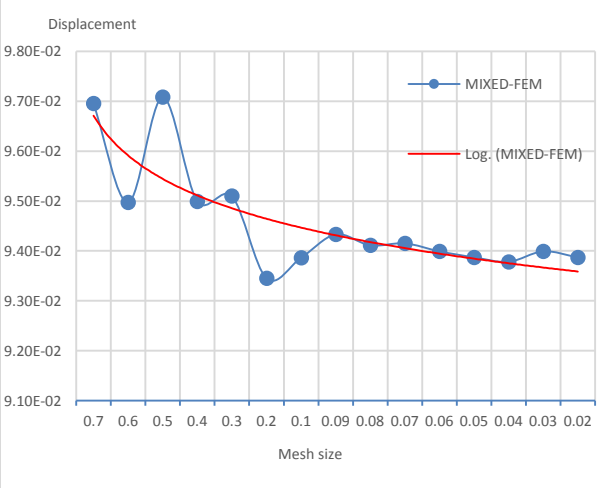


FIG. 11- Convergence rate for Mixed-FEM.

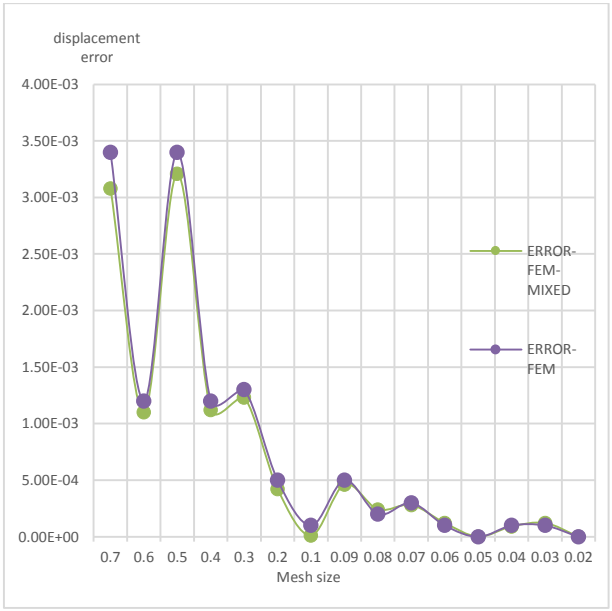


FIG. 12- Error obtained with Mixed-FEM and FEM.

We can calculate the error comparing the results with the reference value; this value corresponds to the finest mesh. This method would allow calculate relative errors in the case where you could not have analytical or experimental results.

$$Er_i = |U_i - U_{ref}|$$

From these tests, we can see that the results of the two methods are very similar with a slight advantage for the mixed finite element methods, based on the results can be observed that for the Mixed-FEM convergence is faster, and more stable from size (0.1).

## 6.2. Numerical test 2: stress intensity factor

Any study of fracture mechanics must analyze the stress intensity factor, which is important for the characterization of the status of cracking and chances of its spread. In this study, we will compare the results of two methods, the standard finite element and mixed finite element. For this, we will compare important results for fracture mechanics including stress intensity factor.

For the numerical test, we will study the impact of the length of the crack on a plate, using both FEM and FEM Mixed-methods, the goal is to calculate the stress intensity factor for each case and compare two methods with analytical approximations.

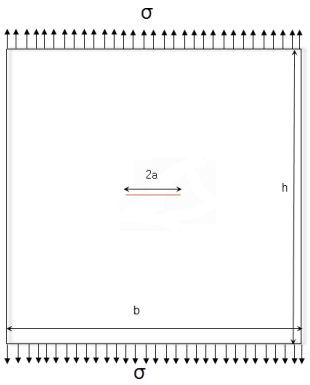


| | |
|---|---|
| h | 10 |
| b | 10 |
| 2a | 0.5 to 4 |
| σ | 1 (SI) |
| Material | |
| Young's modulus | 100 (SI) |
| Poisson's ratio | 0.3 |

FIG. 13- Numerical test data.

## Results

| | FEM (a=2) | MIXED-FEM (a=2) |
|---|---|---|
| $\sigma_{yy}$ | 3.998 (SI) | 3.463 (SI) |
| $\sigma_{xy}$ | 0.897 (SI) | 0.872 (SI) |
| $U_{yy}$ | 0.106 (SI) | 0.106 (SI) |

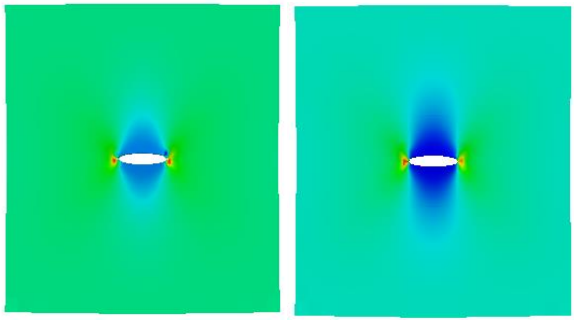

FIG. 14- Stress σyy By Mixed Finite Element Method (Left) And Stress Solution (Right).

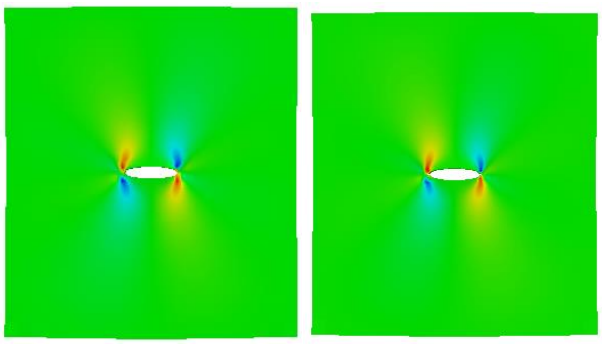

FIG. 15- Stress $\sigma_{xy}$ By Mixed Finite Element Method (Left) And Stress Solution (Right)

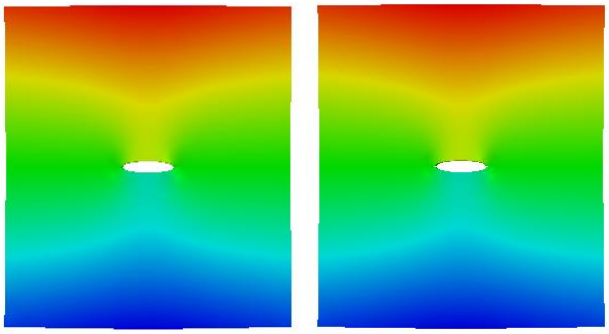

FIG. 16- Displacement Uyy by Mixed Finite Element Method (Left) And Displacement Solution (Right).

To calculate the stress intensity factor approximating **[25]** is used in the case of a cracked plate subjected to a longitudinal tension. we replace in the formula **(53)** $\boldsymbol{fj}$ by :

$$\boldsymbol{f_I = \sqrt{sec\frac{\pi.a}{2.b}}} \qquad \textbf{(58)}$$

we obtain:

$$\boldsymbol{K_I = \sigma\sqrt{\pi.a}\sqrt{sec\frac{\pi.a}{2.b}}} \qquad \textbf{(59)}$$

| Crack | KI-Analytic | KI-FEM | Error % - FEM | KI-MIXED-FEM | Error % MIXED-FEM |
|---|---|---|---|---|---|
| 0.5 | 0.887745028 | 0.684745789 | 29.64592746 | 0.70735 | 25.50293747 |
| 1 | 1.257937058 | 0.845924497 | 48.70559521 | 0.853465 | 47.39175685 |
| 1.5 | 1.543698435 | 1.049740196 | 47.05528487 | 1.062815 | 45.24620323 |
| 2 | 1.786043483 | 1.238281727 | 44.23563268 | 1.255159617 | 42.29612392 |

| | | | | | |
|---|---|---|---|---|---|
| 2.5 | 2.00082 6901 | 1.42 2635 079 | 40.6423 1449 | 1.44419 2529 | 38.5429 4782 |
| 3 | 2.19616 4798 | 1.61 0395 432 | 36.3742 5662 | 1.63664 8417 | 34.1867 1818 |
| 3.5 | 2.37686 9965 | 1.80 5631 757 | 31.6364 7327 | 1.83682 4179 | 29.4010 6042 |
| 4 | 2.54607 2873 | 2.01 0840 893 | 26.6173 2125 | 2.02146 | 25.9521 7681 |

**Table 1**. Comparison of K1-FEM, K1-Mixed and K1-Analytical with different length of crack.

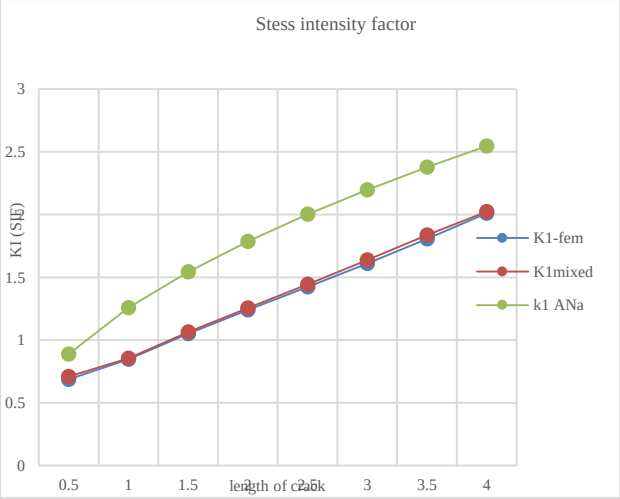


FIG. 17- The Stress Intensity Factor computed with Analytical, Mixed-FEM And FEM methods.

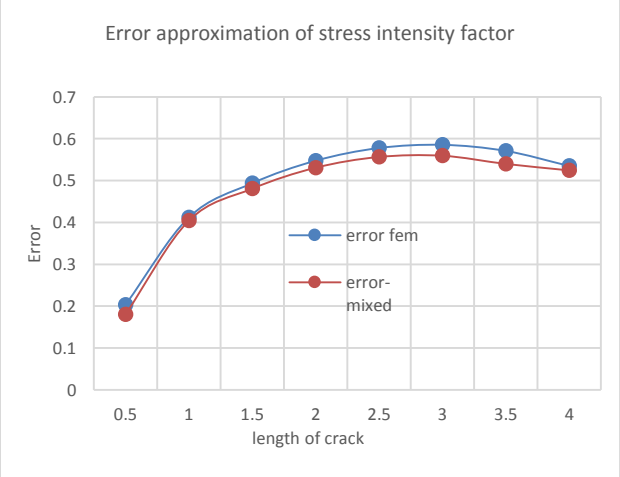


FIG. 18- The Error-SIF computed for Mixed-FEM And FEM methods.

From these results we can conclude that the Mixed-FEM not only gives good results, but slightly more accurate than the conventional method FEM results. we chose to compare the stress intensity factors, given its importance in the field of linear fracture mechanics. present results demonstrate that with the mixed method could increase the accuracy of the results for more complex cases, and avoid too high safety factors in the design of product susceptible to crack propagation

## 7.Conclusion

In this paper we have presented a mixed finite element method for the simulation of a propagating crack under linear elastic conditions. It includes algorithms for discretization by mixed finite element methods. There is a member of the family for each polynomial degree, beginning with degree two for the stress and degree one for the displacement, and each is stable and affords optimal order approximation.

Numerical results are presented to see the performance of the method, and seem to be interesting by comparing them with other recent results.

**Acknowledgements:** The authors would like to appreciate the referees for giving us the several corrections.

**References:**

**[1]** F. Brezzi, J. Douglas, M. Fortin, L. Marini. Efficient rectangular mixed finite elements in two and three ariables, RAIRO Model. Math. Anal. Numer. 21 (3) (1987), 581-604.

**[2]** W. Qiu and L. Demkowicz. Mixed hp-finite element method for linear elasticity with weakly imposed symmetry: stability analysis, SIAM J. Numer. Anal. 49 (2011), no. 2, 619-641.

**[3]** J. Guzman. A unified analysis of several mixed methods for elasticity with weak stress symmetry, J. Sci. Comput., 44 (2010), 156-169.

**[4]** D.N. Arnold, J. Douglas Jr., C.P. Gupta. A family of higher order mixed finite element methods for plane elasticity, Numer. Math., 45 (1984), 1-22.

**[5]** C. Johnson and B. Mercier. Some equilibrium finite element methods for two-dimensional elasticity problems, Numer. Math., 30 (1978), 103-116.

**[6]** F. Brezzi, M. Fortin. *Mixed and Hybrid Finite Element Method*. Springer Verlag; New York, 1991.

**[7]** Douglas N. Arnold, Jim Douglas, Jr., and Chaitan P. Gupta. A Family of Higher Order Mixed Finite Element Methods for Plane Elasticity. Numer. Math. 45 (1984), 1-22.

**[8]** F. Brezzi. On the existence uniqueness and approximation of saddle point problems arising from Lagrangian multipliers, RAIRO 8-32 (1974), 129-151.

**[9]** Douglas N. Arnold and Richard S. Falk. A new mixed formulation for elasticity, Numer. Math. 53 (1988), no. 1-2, 13-30.

**[10]** Vernon B. Watwood Jr. and B. J. Hartz. An equilibrium stress field model for finite element solution of two-dimensional elastostatic problems, Internat. Solids and Structures, 4 (1968), 857-873.

**[11]** Claes Johnson and Bertrand Mercier. Some equilibrium finite element methods for two-dimensional elasticity problems, Numer. Math. 30 (1978), no. 1, 103-116.

**[12]** Douglas N. Arnold, Jim Douglas, Jr., and Chaitan P. Gupta. A family of higher order mixed finite element methods for plane elasticity, Numer. Math. 45 (1984), no. 1, 1-22. MR 761879. (86a:65112)

**[13]** Douglas N. Arnold and Ragnar Winther. Mixed finite elements for elasticity, Numer. Math. 92 (2002), no. 3, 401-419. MR 1930384 (2003i:65103).

**[14]** Shao-Chun Chen and Ya-Na Yang. Conforming rectangular mixed finite elements for elasticity, Journal of Scientific Computing 47 (2010), no. 1, 93-108. MR 2804836 (2012e:74013).

**[15]** Douglas N. Arnold and Gerard Awanou. Rectangular mixed finite elements for elasticity, Math. Models Methods Appl. Sci. 15 (2005), no. 9, 1417-1429. MR 2166210 (2006f:65112).

**[16]** Douglas N. Arnold, Gerard Awanou, and Ragnar Winther. Finite elements for symmetric tensors in three dimensions, Math. Comp. 77 (2008), no. 263, 1229-1251. MR 2398766 (2009b:65291).

**[17]** Scot Adams and Bernardo Cockburn. A mixed finite element method for elasticity in three dim ensions, J. Sci. Comput. 25(2005), no. 3, 515-521. MR 2221175 (2006m:65251).

**[18]** Douglas N. Arnold and Ragnar Winther. Mixed finite elements for elasticity, submitted to Numer. Math. 2001.

**[19]** Douglas N. Arnold, Franco Brezzi, and Jim Douglas, Jr., PEERS: a new mixed finite element for plane elasticity, Japan J. Appl. Math. 1 (1984), no. 2, 347-367.

**[20]** Douglas N. Arnold and Franco Brezzi. Mixed and nonconforming finite element methods: implementation, postprocessing and error estimates, Math. Modelling and Numer. Anal. 19 (1985), 7-32.

**[21]** S. Rahman, F.W. Brust. Approximate methods for predicting J-integral of a circumferentially surfacecracked pipe subject to bending, International Journal of Fracture, Vol 85, 1997, P: 111-130.

**[22]** R.C. Rice, G.F. Rosengren. Plane strain deformation near a crack tip in a power-law hardening material, Journal of Mechanics and Physics of Solids, 16, P 1-12,1968.

**[23]** J.R Rice, G. F. Rosengren. A path independent integral and the approximate analysis of strain concentration by notches and cracks, ASME Journal ofApplied Mechanics, 35, P379-386, 1980.

**[24]** Shih, C. F., B. Moran, and T. Nakamura, " Energy Release Rate along a Three-Dimensional Crack Front in a Thermally Stressed Body," International Journal of Fracture, vol. 30, pp. 79–102, 1986.

**[25]** Tada H., Paris P., I Rwin G. (1973). The stress analysis of cracks handbook. Tech. rep., Del.Research Corporation, Hellertown, Pennsylvania, USA.